NATIONAL RESEARCH COUNCIL OF CANADA

AERONAUTICAL REPORT
LR-500

# A FLIGHT INVESTIGATION OF VARIOUS STABILITY AUGMENTATION SYSTEMS FOR A JET-LIFT V/STOL AIRCRAFT (HAWKER-SIDDELEY P1127) USING AN AIRBORNE SIMULATOR

BY
D. M. McGREGOR
NATIONAL AERONAUTICAL ESTABLISHMENT



OTTAWA
FEBRUARY 1968



NRC NO. 10257

# A FLIGHT INVESTIGATION OF VARIOUS STABILITY AUGMENTATION SYSTEMS FOR A JET-LIFT V/STOL AIRCRAFT (HAWKER-SIDDELEY P1127) USING AN AIRBORNE SIMULATOR

by

D. M. MCGREGOR

A. D. Wood, Head
Flight Research Section

F. R. Thurston
Director

BLANK PAGE

## SUMMARY

A flight investigation of various stability augmentation systems for the Hawker-Siddeley P1127 jet-lift V/STOL aircraft, using a variable stability helicopter, is reported. The main emphasis was placed on overcoming the directional divergence due to the unstable weathercock stability that occurs at low airspeeds, but short investigations of a roll stabilizer to reduce the pilot work load, and a pitch stabilizing device to assist the pilot to maintain attitude in the presence of an angle-of-attack instability, were included. Both visual and a limited number of simulated instrument flights were conducted. After testing several stabilizing devices, it was concluded that a lateral accelerometer operating through the yaw reaction controls yielded directional handling qualities in the "acceptable-satisfactory" region.

TABLE OF CONTENTS


| | Page |
|---|---|
| SUMMARY | (iii) |
| TABLE | (v) |
| ILLUSTRATIONS | (v) |
| SYMBOLS | (vi) |
| 1.0 INTRODUCTION | 1 |
| 2.0 DESCRIPTION OF THE SIMULATOR | 2 |
| 3.0 EQUATIONS OF MOTION | 4 |
| 3.1 Reference System and Sign Convention | 4 |
| 3.2 Conversion of Stability Derivatives from Non-Dimensional to Dimensional Forms | 4 |
| 3.3 Longitudinal Motions | 6 |
| 3.3.1 Longitudinal Force | 7 |
| 3.3.2 Normal Force | 8 |
| 3.3.3 Pitching Moment | 8 |
| 3.4 Lateral-Directional Motions | 9 |
| 3.4.1 Rolling Moment | 9 |
| 3.4.2 Yawing Moment | 10 |
| 4.0 STABILITY AUGMENTATION SYSTEMS | 11 |
| 4.1 Roll Stabilizer | 11 |
| 4.2 Directional Stabilizing Systems | 12 |
| 4.2.1 Yaw Rate Damping Plus "Leaky" Heading Hold | 12 |
| 4.2.2 Sideslip Vane | 12 |
| 4.2.3 Lateral Accelerometer | 13 |
| 4.2.4 Favourable Aileron Yaw | 14 |
| 4.3 Pitch Stabilizer | 14 |
| 5.0 FLIGHT TASK | 15 |
| 5.1 Visual Task | 15 |
| 5.2 Instrument Task | 15 |
| 6.0 RESULTS AND DISCUSSION | 16 |
| 6.1 Roll Stabilizer | 16 |

TABLE OF CONTENTS (Cont'd)


| | | Page |
|---|---|---|
| 6.2 | Directional Stabilizing Systems | 17 |
| 6.3 | Stability Augmentation System Failures | 19 |
| 6.4 | Pitch Stabilizer | 20 |
| 7.0 | CONCLUSIONS | 20 |
| 8.0 | ACKNOWLEDGMENTS | 21 |
| 9.0 | REFERENCES | 21 |


TABLE


| Table | | Page |
|---|---|---|
| 1 | Dimensional Stability Derivatives for the Hawker P1127 | 23 |


ILLUSTRATIONS


| Figure | | Page |
|---|---|---|
| 1 | Airborne V/STOL Simulator | 25 |
| 2 | Basic P1127 Lateral-Directional Modal Characteristics | 26 |
| 3 | "Model-Controlled" Simulation Method | 27 |
| 4 | Power Spectrum of Synthetic Turbulence Generator | 28 |
| 5 | Instrument Panel Arrangement for Visual Flights | 29 |
| 6 | Cockpit Lay-Out for Instrument Flights | 30 |
| 7 | Orange Sub-Cockpit Installation | 31 |
| 8 | Analogue Circuit for the P1127 Longitudinal Equations of Motion | 32 |
| 9 | Analogue Circuit for the P1127 Lateral-Directional Equations of Motion | 33 |

## SYMBOLS

| Symbol | Definition |
|---|---|
| a | Acceleration, $ft/sec^2$ |
| b | Span of airplane, ft |
| $\bar{c}$ | Standard mean chord, ft |
| C | NASA non-dimensional coefficient |
| g | Acceleration of gravity, $ft/sec^2$ |
| $I_A$ | Rolling moment of inertia about stability axes, $slug\text{-}ft^2$ |
| $I_B$ | Pitching moment of inertia about stability axes, $slug\text{-}ft^2$ |
| $I_C$ | Yawing moment of inertia about stability axes, $slug\text{-}ft^2$ |
| $I_E$ | Product of inertia about stability axes, $slug\text{-}ft^2$ |
| IC | Initial condition |
| K | Gain term in turbulence and SAS equations |
| $\ell$ | Characteristic length, ft (longitudinal = $\frac{\bar{c}}{2}$, lateral = $\frac{b}{2}$) |
| L | Rolling acceleration derivative, acceleration per unit subscript. $rad/sec^2$/unit subscript |
| M | Pitching acceleration derivative, acceleration per unit subscript, $rad/sec^2$/unit subscript |
| N | Yawing acceleration derivative, acceleration per unit subscript, $rad/sec^2$/unit subscript |
| p | Angular velocity in roll referred to body-fixed reference axes, rad/sec |
| P | Angular velocity in roll referred to stability axes, rad/sec |
| q | Angular velocity in pitch, rad/sec |
| r | Angular velocity in yaw referred to body-fixed reference axes, rad/sec |
| R | Angular velocity in yaw referred to stability axes, rad/sec |

SYMBOLS (Cont'd)

| Symbol | Definition |
|---|---|
| S | Wing area, $ft^2$ |
| s | Laplace operator |
| SAS | Stability augmentation system |
| t | Time constant, sec |
| u | Perturbation of longitudinal velocity, ft/sec |
| $v_c$ | Velocity vector of airplane mass centre, ft/sec |
| x | Distance along the longitudinal axis, ft |
| X | Longitudinal acceleration derivative per unit subscript, $ft/sec^2$/unit subscript |
| Y | Lateral acceleration derivative per unit subscript, $ft/sec^2$/unit subscript |
| Z | Normal acceleration derivative per unit subscript, $ft/sec^2$/unit subscript |
| | and |
| | Gain of "Leaky attitude" term in SAS transfer functions |
| z | Distance along the normal axis, ft |
| $\alpha$ | Perturbation of angle of attack, rad |
| $\beta$ | Angle of sideslip, rad |
| $\delta$ | Pilot's control deflection, in |
| $\Delta$ | Partial derivative |
| $\zeta$ | Yaw nozzle deflection, deg |
| $\eta$ | Pitch nozzle deflection, deg |
| $\theta$ | Perturbations of pitch attitude, rad |
| $\rho$ | Density of air, $slug/ft^3$ |
| $\xi$ | Roll nozzle and aileron control surface deflection, deg |
| $\omega$ | Frequency, rad/sec |

SYMBOLS (Cont'd)

| Symbol | Definition |
|---|---|
| Subscripts | |
| a | Pilot's roll (aileron) control |
| $a_y$ | Lateral acceleration, $ft/sec^2$ |
| $a_z$ | Normal acceleration, $ft/sec^2$ |
| e | Pilot's pitch control |
| E | Engine |
| g | Gust |
| m | Pitching moment |
| o | Steady-state trimmed condition |
| r | Pilot's yaw (rudder) control |
| T | Thrust |
| $\dot{\alpha}$ | Rate of change of angle of attack perturbation, rad/sec |
| Superscript | |
| ' | Denotes reaction control term |

# A FLIGHT INVESTIGATION OF VARIOUS STABILITY AUGMENTATION SYSTEMS FOR A JET-LIFT V/STOL AIRCRAFT (HAWKER-SIDDELEY P1127) USING AN AIRBORNE SIMULATOR

## 1.0 INTRODUCTION

This program to investigate the handling qualities of a variety of stability augmentation systems for the Hawker-Siddeley P1127 jet-lift V/STOL aircraft was accomplished by a co-operative effort between the Aero Flight Division of the Royal Aircraft Establishment, Bedford, England, and the National Aeronautical Establishment, Ottawa, Canada. The main emphasis was placed on overcoming the directional divergence due to the unstable weathercock stability that occurs at low airspeeds, but the flight program, using a variable stability helicopter (Fig. 1), included short investigations of a roll stabilizer to reduce the pilot work load, and a pitch-stabilizing device to relieve the pilot of the very onerous task of maintaining pitch attitude and, hence, airspeed in the presence of an angle-of-attack instability. The directional instability results from the changes of momentum that take place at the intakes to the engine, which are located well forward of the aircraft centre of gravity, while the pitch instability is due mainly to interference effects of the deflected jet on the tail plane. An indication of the need for improved stability is contained in the Report on the operational evaluation of the Kestrel aircraft, a derivative of the P1127, in which it was shown (Ref. 1) "... that the Kestrel was capable of certain instrument operations without stability augmentation; however, to assure full instrument capability better stability is a requisite."

This lack of adequate stability at speeds less than 120 knots is illustrated by the curves of Figure 2, which show the characteristics of the lateral-directional modes of motion of the P1127 as estimated by the Royal Aircraft Establishment and simulated during these trials. It is seen that below approximately 75 knots the damping of the Dutch Roll mode is negative, causing severe handling difficulties to the pilot.

Preliminary work to estimate and measure the aircraft's stability derivatives, and an analogue computer program to indicate the most useful range of stabilizing parameters to be investigated in flight, were completed by the Royal Aircraft Establishment before the flight tests were begun. References 2 and 3 describe the overall program, while this Report outlines, in greater detail, the portion of the experiment utilizing the airborne simulator.

The following Sections outline the capabilities of the simulator, the conversion of the estimated stability derivatives from their non-dimensional to their dimensional forms as used on this simulator, the parameters tested, the flight tasks undertaken, and the results obtained.

## 2.0 DESCRIPTION OF THE SIMULATOR

The variable stability equipment and the simulation capabilities of this helicopter are described in Reference 4, and Figure 1 shows an overall view of the vehicle. A brief description of the system, and how it was adapted to this problem, follows.

The model-controlled method (Ref. 5) is employed to force the helicopter to follow the motions of the aircraft being simulated, as calculated by the equations of motion set on the analogue computer (Fig. 3). Although the pilot conducting the evaluations controls all motions while airborne, the helicopter is forced to assume only the yaw, roll, pitch, and heave behaviour of the analogue model. The longitudinal and lateral force characteristics of the simulator cannot be altered independently, which meant, for this program, that changes in the direction of the thrust vector normally resulting from changing engine nozzle positions could not be simulated. Consequently, the flight task was representative of fixed nozzle, varying engine rpm slow approaches.

The schematic drawing of Figure 3 indicates how the electrical signals, generated by movements of the evaluation pilot's controls and by various aircraft sensors, such as the vanes measuring angles of attack and sideslip, are used as inputs to the analogue computer. Random electrical signals shaped and scaled to simulate low level turbulence can be introduced to disturb the simulator, providing more realistic flight conditions. The shape of the power spectrum of the three turbulence components used in the investigation appears in Figure 4. Each was scaled to represent rms gust velocities of 6 ft/sec.

The computing equipment available for setting up the model consists of 56 operational amplifiers, 26 integrating or non-linear components, 12 function switches, 46 gain-setting potentiometers, and other miscellaneous components. Twenty of the gain-setting potentiometers and all the function switches are in the cockpit, conveniently located to allow either pilot to alter the settings. This capability was used to advantage during the program: (i) to adjust some of the estimated stability derivatives to make

the simulator fly like the actual aircraft (see Sect. 3.3), and (ii) to investigate rapidly a variety of proposed lateral-directional stability augmentation systems. The reliability of both the helicopter and the simulation equipment was demonstrated by the 23 research sorties, totalling more than 23 hours of flight time, that were accomplished in 10 days.

A 14-channel oscillograph flight recorder was used to document the calculated and actual rolling and yawing angular rates, pilot and SAS control inputs, lateral accelerations, and sideslip angles during each evaluation manoeuvre.

Both visual and a limited number of simulated instrument flights were conducted. The instrument panel arrangement of Figure 5 was used for the visual flights and was altered to that of Figure 6 for the instrument approaches. An attempt was made to reproduce the pilot's view of the landing site by blanking off portions of the cockpit. During the instrument flying the pilot wore blue goggles, and an orange subcockpit was inserted (Fig. 7) to preclude his use of external visual clues. Simulated flight instruments were added to indicate percent engine rpm and the angles of attack and sideslip. These latter two assume the role of primary flight instruments because of the longitudinal and directional instabilities, while the angle-of-attack vane is required also to allow the pilot to optimize the transition procedure of the real aircraft. A synthetic ILS similar to the one described in Reference 6 provided a convenient and appropriate aid for the instrument approach task.

Two pilots occupied the aircraft during all tests, with the one on the left acting as safety pilot while the one on the right evaluated the handling qualities of the various combinations investigated. All the flying during the evaluation of the lateral-directional characteristics was accomplished by one pilot from RAE, Bedford, who had been project pilot on the P1127 for several years and had flown over 45 hours on the various versions of that aircraft. Several flights were made subsequently to investigate the advantages of a pitch stabilizer. During these flights five other pilots, only one of whom had flown the P1127, participated.

The control feel for the evaluation pilot's control column and rudder pedals was produced by a spring system with viscous damping, while the "power lever" had adjustable friction only. The spring gradients were held constant at $1\frac{1}{2}$, $1\frac{1}{4}$, and 10 lb/in for the pitch, roll, and directional controls respectively, and were judged to

be representative of the control column forces of the real aircraft, but approximately one-half the pedal forces. The maximum control throws were the same as for the real aircraft.

## 3.0 EQUATIONS OF MOTION

### 3.1 Reference System and Sign Convention

Since the pilot attempts to fly the P1127 at an angle of attack of 8 degrees during low speed approaches, the derivatives supplied by the RAE from flight data or from theoretical estimates were computed about stability axes depressed by this angle from the longitudinal reference line of the aircraft. The stability augmentation system transducers in the aircraft are aligned, however, with body-fixed axes. Since the airborne simulator's reference system is body-fixed, aligned with the rate gyros, all computed motions were ultimately resolved along the set of axes containing the stability augmentation system transducers of the P1127 before being used by the simulation system. Following this resolution the calculated motions were compared with the simulator's motions, as indicated in Figure 3; hence, the simulator's reference axes became the body-fixed reference axes of the P1127.

The sign convention used with the simulator is the same as the NASA system (Ref. 7), with the exception of the direction of control movements. In the notation used here, positive longitudinal and lateral pilot's stick motion and positive pilot's rudder motion produce positive angular accelerations (i. e. nose-up, right roll, and right yaw).

### 3.2 Conversion of Stability Derivatives from Non-Dimensional to Dimensional Forms

The stability derivatives were first derived in the NASA non-dimensional form (Ref. 7) and then converted to the dimensional derivatives normally used with this simulator. All contributions were accounted for in these terms, including the basic aircraft characteristics plus the destabilizing intake momentum contributions assuming an rmp setting of 95 percent.

The following example illustrates the process by showing the conversion of one derivative, $C_{m_\eta}$, the non-dimensional pitching moment coefficient resulting from a deflection of the elevator control surface, to $M_{\delta_e}$, the pitching acceleration resulting

from movements of the pilot's pitch control $\left(\frac{\text{rad/sec}^2}{\text{in}}\right)$.

The non-dimensional pitching moment coefficient is

$$C_m = \frac{M}{\rho v_c^2 S \ell}$$

Each term is defined in the list of symbols. The dimensional derivative, $M_{\delta_e}$, is

$$M_{\delta_e} = \frac{1}{I_B} \frac{\Delta M}{\Delta \delta_e}$$

Hence,

$$M_{\delta_e} = \frac{1}{I_B} \frac{\Delta (C_m \rho v_c^2 S \ell)}{\Delta \delta_e}$$

$$= \frac{\rho u_o^2 S \ell}{I_B} \frac{\Delta C_m}{\Delta \delta_e}$$

$$= \frac{-\rho u_o^2 S \ell}{I_B} \frac{\Delta C_m}{\Delta \eta} \cdot \frac{\Delta \eta}{\Delta \delta_e}$$

$$= -\left\{ \frac{\rho u_o^2 S \bar{c}}{2 I_B} \frac{\Delta \eta}{\Delta \delta_e} \right\} C_{m_\eta}$$

since $\ell = \frac{\bar{c}}{2}$ for the longitudinal derivatives and

$$\frac{\Delta C_m}{\Delta \eta} = C_{m_\eta}$$

(See Sect. 3.1 for an explanation of the sign change.)

The quantity inside the large bracket above, then, is the conversion factor from the non-dimensional to the dimensional derivative and is a function of the physical characteristics of the P1127 (e.g. $I_B$, $\bar{c}$, S, and the control system gearing, $\frac{\Delta \eta}{\Delta \delta_e}$)

and the flight conditions (e. g. $\rho$, $u_o$). Each of the derivatives was converted in a similar fashion for two airspeeds, 50 and 80 knots, yielding the dimensional values shown in Table 1. It should be noted that both the weathercock stability, $N_\beta$, and the pitching moment due to changes of angle of attack, $M_\alpha$, are unstable, producing a very difficult handling problem for the pilot. The task undertaken in this program was the correction of these deficiencies by a system to augment the stability.

3.3 Longitudinal Motions

Although only two modes of longitudinal motion are controlled by the variable stability system (the pitch rate and the normal acceleration), the motion in the other degree of freedom, the longitudinal velocity, was calculated and used to modify the other two modes in an appropriate manner. For example, when the nose of the aircraft was depressed, the equations of motion set on the analogue computer calculated the increase in longitudinal velocity that the P1127 would experience, and this velocity in turn influenced the pitching and heaving motions that were duplicated by the simulator.

It was found necessary to alter the level of two of the longitudinal derivatives, $M_\alpha$ and $Z_{\delta_T}$, the changes of pitching acceleration with angle of attack, and the normal acceleration with throttle input, to make the simulator fly more like the actual aircraft. The final values appear in Table 1. The required alteration of $M_\alpha$ probably was due to difficulties in estimating this term, while the change in $Z_{\delta_T}$, which was increased threefold, resulted from an inherent deficiency of the simulator, which is incapable of providing longitudinal force variations independent of rotor tilt. This latter deficiency showed up most emphatically when attempting to overshoot from a landing approach by applying power. When the simulator started to ascend, the angle of attack would decrease sharply from the 8-deg level indicated on the approach to approximately zero, causing a large calculated downward force through the $Z_\alpha$ term. The 8-deg angle of attack could not be maintained on the climb-out, as it is on the P1127, because the pitch attitude of the simulator could not be increased without drastically decreasing the airspeed. The changes resulted in handling qualities similar to those experienced on a "nozzle-fixed" approach with the real airplane. Since the overshoot was not an essential part of the task used in this evaluation, lack of realism in reproducing this manoeuvre was not considered important compared with the perturbation characteristics that were reliably reproduced during the approach task.

All the equations described below were properly scaled and programmed on the analogue computer (Fig. 8, 9) to comprise the "model" of the simulation system.

Limits were imposed on the simulated controls both by physically restricting the control throws available to the pilot to those of the actual aircraft, and by limiting the voltages in various locations to duplicate the deflections of the reaction control nozzles.

3.3.1 Longitudinal Force

The equation adequately describing the perturbations in the inertial longitudinal acceleration was

$$\frac{du}{dt} = x_u(u+u_g) + x_\alpha(\alpha+\alpha_g) - g\theta$$

since $\cos \theta_o \approx 1$. The term required for use in the other two longitudinal equations was the perturbation velocity; hence, the following equation combining the inertial velocity with the gust velocity actually was used in the calculation as shown in the circuit diagram of Figure 8.

$$u + u_g = X_u \int (u+u_g)\, dt + X_\alpha \int (\alpha+\alpha_g)\, dt - g \int \theta\, dt + u_g$$

It will be noted that a vertical gyro was used, together with a "signal cancelling" network, to obtain the perturbation values of the pitch angle, $\theta$. Similar circuits, which make it possible to start any given signal at an effective zero level, representing the trimmed condition, and to measure perturbations, were used also with the angle of attack and lateral accelerometer signals as shown in Figures 8 and 9.

The angle-of-attack vane is mounted on the skid of the helicopter, as shown in Figure 1, ahead of and to the left of the centre of gravity. Hence, its readings were corrected for roll and pitch angular rates before being used in the calculations. The initial angle-of-attack indication to the pilot was 8 deg, and perturbations about this were calculated after the evaluation pilot took control.

A random electrical noise signal, shaped to the power spectrum of Figure 4 and scaled to represent a longitudinal gust velocity of 6 ft/sec rms, was available. Similar independent turbulence generators simulated angle-of-attack and sideslip

disturbances due to vertical and lateral gusts and were scaled to represent rms angle deflections corresponding to rms gust velocities of 6 fps at the speeds flown. All the synthetic turbulence signals could be switched in and out by actuating switches in the cockpit To achieve flight conditions representative of moderate turbulence, only the lateral noise generator was utilized for the majority of the tests.

3.3.2 Normal Force

The normal acceleration experienced by an aircraft is a function of the aerodynamic forces, including the propulsive forces, acting on it. Hence, the equation describing the perturbations in the normal acceleration and used to construct the appropriate part of the model was

$$a_z = Z_u(u+u_g) + Z_\alpha(\alpha+\alpha_g) + Z_{\delta_T} \cdot \delta_T + Z_{\delta_e} \cdot \delta_e$$

Figure 8 illustrates how various transducers were used to obtain electrical signals proportional to the above parameters.

The dynamics of the engine were simulated initially by a first-order system having a time constant of 0.7 sec as shown, but, since the pilot complained that decreases in thrust were achieved too slowly, this feature was deleted after the second flight.

The locations in the circuit where the pilot's indications of engine rpm and angle of attack were obtained are shown in Figure 8.

3.3.3 Pitching Moment

Since the simulator utilizes the angular velocity in pitch as one of the signals controlling the high gain autopilot, the pitching equation of motion was programmed on the analogue computer to yield a signal proportional to the pitching rate. Then the equation of motion was

$$q = M_{\delta_e} \int \delta_e \, dt + M_{\delta_e'} \int \delta_e' \, dt + Mq \int q \, dt$$

$$+ M_u \int (u+u_g) \, dt + M_\alpha \int (\alpha+\alpha_g) \, dt + M_{\dot\alpha} \int (\dot\alpha+\dot\alpha_g) \, dt$$

Since, by this method, the $\dot{\alpha}$ term was integrated, there was no necessity to differentiate the $\alpha$ signal; rather it was used directly as shown in Figure 8.

The limits of travel of the reaction control nozzles were reached before those of the aerodynamic control surfaces and were set by the diode networks shown.

3.4 Lateral-Directional Motions

Since this simulator is incapable of modifying the side force characteristics of the helicopter to match those of the vehicle being simulated, and since the pilot is aware of side force perturbations through both "the seat of his pants" and the flight instruments such as the ball indicating "slip and skid", the actual sideslip of the simulator as measured by the sideslip vane was accepted and used in the rolling and yawing equations of motion.

3.4.1 Rolling Moment

It is common practice with this simulator to convert all the angular equations of motion to forms that calculate the angular rates rather than the angular accelerations. However, since it was desired to simulate the placement of the lateral accelerometer at various practical positions in the P1127, somewhat modified rolling and yawing angular accelerations were derived to allow these simulated movements of the accelerometer to be effected. As is seen in Figure 9, the angular velocities were ultimately computed as required by the simulation system.

The equation describing the rolling motion about the stability axes depressed 8 deg to the fuselage longitudinal reference line was

$$\frac{dP}{dt} = L_{\delta_a} \cdot \delta_a + L_{\delta_a'} \cdot \delta_a' + L_{\delta_r} \cdot \delta_r + L_{\delta_r'} \cdot \delta_r' + L_P \cdot P + L_R \cdot R$$

$$L_\beta \cdot (\beta+\beta_g) + \frac{I_E}{I_A} \frac{dR}{dt}$$

The last term of this expression was used in the calculation of the rolling angular velocity, where the differential disappears, but was excluded in the computation of the rolling acceleration, causing some error in the acceleration signal.

Resolution of the angular rates from the stability axes to the body-fixed reference axes is described in the following Section.

3.4.2 Yawing Moment

Exactly the same procedure as outlined in the last Section for the rolling motion was used to derive both the angular velocity in yaw and a signal approximating the yawing angular acceleration. The equation used was

$$\frac{dR}{dt} = N_{\delta_r} \cdot \delta_r + N_{\delta_r'} \cdot \delta_r' + N_{\delta_a} \cdot \delta_a + N_{\delta_a'} \cdot \delta_a' + N_R \cdot R$$

$$+ N_p \cdot P + N_\beta \cdot (\beta+\beta_g) + \frac{I_E}{I_C} \frac{dP}{dt}$$

The circuit diagram of Figure 9 indicates how these lateral-directional equations were constructed and yielded signals proportional to the angular velocities in roll and yaw about the stability axes. The rates about body reference axes 8 deg nose-up from the stability axes were required, however, for use by the variable stability system (Sect. 3.1). The equations effecting this conversion from P and R, the angular rates about the stability axes, to p and r, the angular rates about the body-fixed reference axes, are

$$p = P \cos 8° - R \sin 8°$$

$$r = R \cos 8° + P \sin 8°$$

but

$$\cos 8° \approx 1$$

$$\sin 8° = 0.139$$

Therefore

$$p \approx P - 0.139 R$$

$$r \approx R + 0.139 P$$

These expressions were programmed on the analogue computer (Fig. 9) and yielded

signals proportional to p and r, which were used, in turn, by the high gain autopilot as described in Section 2.0.

## 4.0 STABILITY AUGMENTATION SYSTEMS

As was outlined in the Introduction, the object of this research was to develop a satisfactory system to augment the stability of the P1127 jet-lift V/STOL aircraft. Various augmentation features were tested, utilizing signals from a variety of transducers as inputs to the stabilizing systems. Gain-setting potentiometers located in the cockpit allowed a wide range of SAS gains to be investigated readily, while function switches shown in Figures 8 and 9 facilitated selection of the SAS feature to be looked at on any particular approach. This latter feature was particularly useful in highlighting differences between various SAS features, since they could be switched in and out rapidly to illustrate the changes in handling qualities as the evaluation manoeuvres were attempted. Initially the authority of each stabilizing system was limited to 50 percent of the reaction nozzle control power, but this was later reduced to 30 percent to ensure that the pilot could control the effects of hard-over failures in all reasonable flight conditions. Both zero failures, wherein the transducer was assumed to stop functioning and return to zero output, and hard-over failures, which simulated instantaneous failure of the transducer resulting in a maximum transducer voltage output, were tested with the lateral accelerometer and the roll stabilizer described below.

### 4.1 Roll Stabilizer

The P1127 aircraft has been flown for several years and has been successfully piloted through its complete flight envelope and in all flight regimes without the assistance of any form of stability augmentation system. However, to lower the pilot work load by improving the lateral-directional handling qualities, a roll stabilizer operating through both the aileron control surfaces and the reaction nozzles is installed with the following transfer function

$$\frac{\xi}{p} = K_a \left[ 1 + \frac{Z_a}{s + 1/t_a} \right] \cdot \left( \frac{\text{deg aileron}}{\text{deg/sec roll rate}} \right)$$

That is, the aileron control surface deflection is a function of both a pure rate term supplying angular rate damping in roll and a "leaky" attitude hold feature represented

by the $\frac{Z_a}{s + 1/t_a}$ portion of the expression above. The time constant, $t_a$, was held at 5 sec throughout, while $K_a = 0.25$ and $0.01$ were tested with $Z_a = 1.0$ and $2.0$ respectively. Figure 9 illustrates how the calculated roll rate signal simulating the output of the roll gyro of the P1127 was lead through the failure selection circuit and thence into the analogue circuit representing the expression above. Two limits were imposed on the electrical signals in this network. One represented the mechanical limit of the SAS input and the other, set to the same value, limited the electrical output of the leaky attitude term. Similar limits exist in the actual aircraft.

4.2 Directional Stabilizing Systems

4.2.1 Yaw Rate Damping Plus "Leaky" Heading Hold

A system with exactly the same form as the roll device described in the last Section was incorporated in yaw as one possible means of overcoming the directional divergence. As with all the yaw stabilizers outlined below, only the directional reaction nozzle responds to outputs from this system. A portion of Figure 9 illustrates the electrical analogue of the transfer function

$$\frac{\zeta}{r} = K_r \left[1 + \frac{Z_r}{s + 1/t_r}\right], \left(\frac{\text{deg yaw nozzle}}{\text{deg/sec yaw rate}}\right)$$

Because of a computer wiring error, the rate portion of this transfer function was tested initially at a gain 10 times higher than intended. This caused difficulties in turning the simulator that were attributed to the "leaky" heading hold term, and this method of stabilization was rejected. Tests subsequent to finding the error indicated that a small amount of artificial rate damping enhanced the directional characteristics, but insufficient time remained to re-test the "leaky" heading hold feature. Failures of the rate gyro were not simulated, but since the gain found to give acceptable performance was quite low (Sect. 6), no difficulties are anticipated.

Values of $K_r$ ranging from zero to $3.5 \frac{\text{deg}}{\text{deg/sec}}$ were tested.

4.2.2 Sideslip Vane

Yaw reaction nozzle inputs responding in a stabilizing direction and following the control law

$$\frac{\zeta}{\beta} = c, \left(\frac{\text{deg yaw nozzle}}{\text{deg sideslip}}\right)$$

were programmed as shown in Figure 9. Two mounting positions of the sideslip vane were simulated, (i) at the centre of gravity, and (ii) 22.5 ft ahead of the centre of gravity. This latter position is typical of the location on the nose of the actual aircraft. In practice, a vane cannot be mounted at the centre of gravity, of course, but the influences of aircraft motions on a boom-mounted vane can be eliminated, producing the desired effect. The actual sideslip of the helicopter, measured by the vane mounted on the right skid and corrected for helicopter motions, was used as the sensor.

Several values of "C" were tested from zero to 0.3 $\frac{\text{deg}}{\text{deg}}$ for both the simulated positions.

During the tests to simulate the movement of the sideslip vane to the forward position, the vane signal was modified by the addition of an appropriate scaled voltage proportional to the angular rate of yaw, as shown by a solid line in Figure 9. It was not appreciated until later that the aerodynamic terms (viz. the weathercock stability, $N_\beta$, and the dihedral effect, $L_\beta$), which should have continued to receive the centre of gravity sideslip angle in the computer, were receiving the modified signal. The dashed line indicates the wiring as it should have been to supply only the stabilization system with the signal simulating the forward vane mounting position. This resulted in the damping terms $L_R$ and $N_R$ being effectively altered from their values shown in Table 1. $L_R$ became -0.075 at 80 knots and -0.18 at 50 knots rather than +0.24 and +0.084 $\frac{\text{rad/sec}^2}{\text{rad/sec}}$, while $N_R$ became -0.32 at 80 knots and -0.29 at 50 knots rather than -0.31 and -0.25 $\frac{\text{rad/sec}^2}{\text{rad/sec}}$.

It can be safely argued that the change in the directional damping, $N_R$, is insignificant and, since the difficulties experienced by the pilot while testing the forward mounting position of the vane were directional rather than lateral, it would seem that the $L_R$ contribution did not affect the pilot's opinion seriously.

4.2.3 Lateral Accelerometer

The control law tested, relating yaw reaction control inputs resulting from

lateral accelerations was

$$\frac{\zeta}{a_y} = -d, \left( \frac{\text{deg yaw nozzle}}{\text{ft/sec}^2 \text{ lateral acceleration}} \right)$$

and utilized the two lateral accelerometers mounted on the simulator to yield electrical signals proportional to transverse accelerations. Dual accelerometers are used in the helicopter to eliminate acceleration signals due to yawing and rolling manoeuvres. A practical mounting position for a lateral accelerometer on the actual P1127 aircraft is 6 ft aft and 2.5 ft above the centre of gravity; hence, this location was simulated by adding signals proportional to the yawing and rolling angular accelerations and these distances (Fig. 9), as well as the centre of gravity location.

Several values of d from zero to 4.6 $\frac{\text{deg}}{\text{ft/sec}^2}$ were tested at both locations.

4.2.4 Favourable Aileron Yaw

It is a relatively easy undertaking to obtain some positive (favourable) yawing acceleration due to rolling inputs on the P1127 by tilting the roll reaction nozzles rearward. Zero nozzle tilt and approximately 29 deg of tilt angle were programmed in this simulation, as shown in Figure 9, and altered the sign of this term from the basic aircraft's negative value, shown in Table 1, to a positive value of 0.024. (This change should have reduced the roll control sensitivity resulting from the reaction nozzles by approximately 10 percent, but this term was not altered when the favourable yaw was tested.)

4.3 Pitch Stabilizer

During the investigation of the lateral-directional characteristics, and especially during the instrument flying task, it became evident that a large amount of pilot attention had to be devoted to controlling the pitch attitude. Therefore a brief program was conducted with a pitch stabilizer of exactly the same "rate damping plus leaky attitude" form as used in roll. The only transfer function tested was

$$\frac{\eta}{q} = 0.2 \left[ 1 + \frac{2}{s + 0.2} \right], \left( \frac{\text{deg of pitch nozzle}}{\text{deg/sec}} \right)$$

Only the pitch reaction nozzle was actuated by this system and was limited

to an authority of 30 percent. Figure 8 illustrates how this device was simulated.

## 5.0 FLIGHT TASK

The stability derivatives programmed in the equations of motion of the model were set before each flight for either 50 knots or 80 knots, and all approaches for that sortie were made at the appropriate speed. After selecting the desired stabilizing feature at the appropriate gain, the safety pilot climbed the aircraft to approximately 1500 ft above the local terrain, set the airspeed, reduced the engine power to achieve a glide path of approximately 3 to 5 deg terminating in a selected field, manipulated his directional control to set the sideslip to zero as indicated by the evaluation pilot's flight instrument, and requested the evaluation pilot to engage the autopilot and take control by placing the analogue computer in its "operate" mode. The evaluation pilot, who was aware of the SAS feature to be tested, then took control and attempted the manoeuvres described below.

### 5.1 Visual Task

During the visual approaches four separate exercises were attempted to highlight the lateral-directional behaviour. First, the evaluation pilot attempted to maintain the desired approach path using the ailerons only, keeping the rudders fixed. This was essentially a matter of small corrections and straight flight. Then, still using the ailerons only, he executed a typical side step manoeuvre to change the projected touchdown point to a different field. This was essentially a turning manoeuvre and representative of lining up on the approach from a visual circuit, or of a large correction required when becoming visual from an instrument approach. Subsequently, these two tasks were repeated, using aileron and co-ordinated rudder as required. The approach was continued to approximately 5 to 10 ft above ground, when, in the majority of the cases, the safety pilot took control; at other times an overshoot was initiated before the evaluation pilot relinguished control. Similar manoeuvres were performed while briefly assessing the pitch stabilizer.

Comments on each manoeuvre for each of the approximately 160 approached attempted were recorded for discussion following the flight.

### 5.2 Instrument Task

Toward the end of the program, after characteristics for a satisfactory lateral-directional stabilizer had been determined, two flights were made during which

instrument approaches using the equipment described in Section 2.0 were attempted by the evaluation pilot. The glide path was adjusted to 3 deg while its sensitivity was held at the standard ILS value of ±0.5 deg. The localizer was swung to cause all approaches to be made into the surface wind and its sensitivity was set at ±5 deg (one-half the standard value). The decreased localizer sensitivity was found necessary to enable the pilot to obtain sufficient information from it to adequately bracket the localizer beam. This, no doubt, was partially due to the inherent difficulties of this type of low speed instrument flying, but also to the localizer and the glide path emanating from the same point source rather than the localizer being displaced well behind the touchdown point as it is in a normal airport ILS system.

The setting up of the initial conditions for these instrument approaches was similar to that described in the last Section. However, the evaluation pilot was given control while on the localizer in a descent at the proper sink rate (so that the angle-of-attack calculation would start from the proper trimmed condition), but not necessarily on the glide path. He then attempted to guide the aircraft down the ILS beam until approximately 100 ft above ground level, where the safety pilot assumed control and proceeded to climb back up for another approach.

## 6.0 RESULTS AND DISCUSSION

Because of the limited time available for the RAE personnel to spend at this Establishment, a relatively small number of stabilization features, basically those indicating most promise from computer studies, were investigated in flight. These included two roll stabilizer characteristics, a variety of directional stabilizing devices and, after the most acceptable lateral-directional had been determined, one pitch stabilizer.

### 6.1 Roll Stabilizer

The influence of the roll stabilizer without stabilization in yaw was greeted by the pilot with mixed feelings, as is evidenced by his post-trial coments:

"The roll stabilizer currently fitted to the P1127 prototype ($K_a = 0.25$) has a rate damping term together with a leaky attitude term ($Z_a = 1.0$) having a 5-sec time constant. The effect of this stabilizer on the simulation (as on the prototype) was to make the aircraft stable in roll and to increase the stick demands needed

to achieve a given roll rate. Bank angles were easier to hold steady, there was no tendency to overcontrol and, in general, the rolling characteristics were very pleasant indeed. This change had two opposite effects on the directional control characteristics. It could either make it so much easier to control the roll axis that more time and effort was available to control the vital slip angles or, alternatively, the docile roll behaviour led the pilot into rolling manoeuvres which were much more ambitious than when unstabilized and this led to an increase in the directional workload, which sometimes resulted in loss of control. There was no doubt that when used sensibly the roll stabilizer made overall lateral and directional control a little easier. However, this pilot could not make up his mind which he preferred, a light touchy aircraft in roll and yaw or an unharmonized aircraft with an exaggerated directional problem. If anything, when flying a straight approach the stabilizer was preferred but when manoeuvring the harmonized aircraft seemed a little easier to co-ordinate. Turbulence did not seem to alter the relative merits of the systems."

Changing the roll stabilizer characteristics to $K_a = 0.01$ and $Z_a = 2.0$ moved the pilot to comment, "Handling was midway between the original roll stabilizer characteristics and the basic aircraft. The arguments of the previous paragraphs still applied and again turbulence did not cause a change of assessment. Changes in the roll stabilizer characteristics did not result in a compromise between the difficulties of the original roll stabilizer and the basic aircraft; rather they produced handling which seemed to lack the advantage of either extreme."

The original roll stabilizer proved very beneficial when used in conjunction with a variety of directional stabilizing features, however, and was used in the majority of the testing described in the following Section.

## 6.2 Directional Stabilizing Systems

Each stabilization device was investigated separately through the ranges outlined in Section 4, and then various combinations of "best" gains were tested. The combination of sensors and the gains that gave the most satisfactory handling qualities was:

(i) Lateral accelerometer, $d = 3.4 \frac{\text{deg yaw reaction nozzle}}{\text{ft/sec}^2 \text{ lateral acceleration}}$

(ii) Yaw rate, $K_r = 0.25 \frac{\text{deg yaw reaction nozzle}}{\text{deg/sec yaw rate}}$

(iii) Roll nozzle tilt = 29 deg aft

With this stability augmentation the pilot was able to keep the sideslip angle within ±5 deg at the 80-knot approach speed for all the manoeuvres tested. These manoeuvres were considered reasonably demanding for a jet-lift fighter. In fact, acceptable performance was obtained at 80 knots by utilizing the lateral accelerometer only, but the addition of the other two terms enhanced the handling qualities noticeably. At 50 knots no acceptable system was determined, although the rate of divergence was reduced to approximately that of the basic aircraft at the higher flight speed. Because of other factors, such as fuel consumption and engine life, this lower speed seems unlikely to be desirable for operational use and, hence, the main effort was devoted to the 80-knot case.

The influence of the rate gyro and the roll nozzle tilt on the flight characteristics can be expressed in terms of changes in the stability derivatives of Table 1. By applying various factors, such as the gearing between the pilot's rudder pedals and the yaw reaction nozzles and the control sensitivity of the nozzles, the contributions of the "satisfactory" stability augmentation are found to be:

(a) The yaw damping, $N_R$, is increased by $-0.60 \frac{\text{rad/sec}^2}{\text{rad/sec}}$ making it -0.85 at 50 knots and -0.91 at 80 knots.

(b) The aileron yaw, $N_{\delta_a}$, is increased by $0.032 \frac{\text{rad/sec}^2}{\text{in}}$, which is seen from Table 1 to change this derivative from an adverse value of -0.0084 to a favourable level of +0.024.

(The lateral accelerometer's contribution can be put in a similar form yielding $N_{a_y} = 0.12 \frac{\text{rad/sec}^2}{\text{ft/sec}}$.)

The pilot was unable to perceive any difference in the handling qualities due to movement of the lateral accelerometer from the centre of gravity to the more practical aft mounting position (Sect 4. 2. 3).

Results comparable with those obtained with the lateral accelerometer could

be obtained using the sideslip vane hypothetically mounted at the centre of gravity, but moving it forward by 22.5 ft caused a directional oscillation when its gain was high. This was attributed to a substantial decrease in the effective directional rate damping.

Even the effective centre of gravity position was rejected from consideration relatively early in the program since (a) for a practical system a vane is too easily damaged, especially in squadron use, (b) its response to turbulence and, hence, its turbulent input to the stability augmentation system would be higher than that of the lateral accelerometer, and (c) it is of no use in the hover where any side velocity is interpreted as 90 deg of sideslip.

The "leaky" heading hold feature of the yaw stabilizer, as tested, was unacceptable, but no firm conclusions can be reached on its desirability because of the computer wiring error cited in Section 4.2.1. It seems evident, however, that even though this method is very powerful in overcoming the directional instability, it is inherently unacceptable since it increases the amount of attention that the pilot must devote to turn co-ordination. The most desirable method of effecting moderate heading changes during approaches of the type used in this investigation is to have co-ordinated turns result from aileron inputs alone. Conversely, this "leaky" heading hold feature endeavours to keep the heading constant, inducing a sideslip as the aileron is applied, thus requiring the pilot to use his rudders in all turns.

The combination of the roll and directional stabilization characteristics yielded satisfactory lateral-directional handling qualities for both visual and simulated instrument flight, but the pilot encountered difficulties controlling the pitch attitude, particularly during instrument approaches. As is outlined in Section 6.4, the addition of the pitch stabilizer cured this problem.

### 6.3 Stability Augmentation System Failures

An important consideration when incorporating a stability augmentation system in any aircraft is to make sure that the pilot can retain control following any possible failure. Two main effects determine how well he is able to cope: (a) the size of the transient input, and (b) the handling qualities of the aircraft before and after the failure. The size of the transient depends on the manoeuvre being performed and the direction of the failure (as well as the authority of the system, which in the present case was held constant at 30 percent). For example, if the aircraft is in a moderate

banked turn to the right, the roll stabilizer will be hard against its left stop, attempting to roll the aircraft out of the turn. If a "hard-over left" failure now occurs, the pilot will not appreciate it until he starts to roll out of the turn. However, if a "hard-over right" failure occurs he will be rapidly rolled further into the right turn and could be presented with a difficult recovery problem.

Both zero failures, wherein the transducer instantaneously assumed a zero value and stayed there, and hard-over failures, wherein the transducer instantaneously delivered its maximum positive or negative value and held it, were simulated for both the lateral accelerometer and the roll rate gyro. These failures were programmed by the safety pilot and were selected, without warning the evaluation pilot, while he was manoeuvring on the approach. The evaluation pilot was aware, in general, that a failure was to occur sometime on the approach. In no case, even on the occasions when no prior warning was given, did the pilot conducting these trials lose control because of a failure of a stabilization system.

### 6.4 Pitch Stabilizer

The unstable pitching moment due to angle of attack ($M_\alpha$ of Table 1) created a difficult handling qualities problem to the pilot, especially during simulated instrument flight. On several occasions the simulator pitched up and, owing to a limited nose-down control power at the 80-knot approach speed, control was lost and the safety pilot had to disengage the system and recover. To oversome this deficiency, a pitch stabilizer of the form shown in Section 4.3 was installed and tested by five pilots (only one of whom had flown the P1127) during visual approaches. It was the unanimous opinion that this feature improved the handling qualities enormously from a pilot opinion rating (Cooper Rating Scale) of approximately 6 to approximately 2. Unfortunately, the pilot who had done all the flying on the lateral-directional portion of the program was not available to fly this added feature.

## 7.0 CONCLUSIONS

This investivation of a variety of stabilization systems for a jet-lift V/STOL aircraft (P1127) indicates the following:

(i) Satisfactory directional handling qualities can be obtained through a stabilization system employing a lateral accelerometer as the sensing transducer

operating the yaw reaction nozzle with an authority limited to 30 percent of full control.

(ii) Similar results can be obtained in forward flight through a sideslip vane but, because of practical considerations of operational use, such a device would probably be difficult to maintain. In addition, a vane could not be utilized in hovering flight.

(iii) The handling qualities can be enhanced further by the addition of a stabilizing term that increases the directional angular rate damping (using a rate gyro as the sensing element) and by increasing the favourable yaw due to aileron input (making it positive by tilting the roll reaction nozzles aft).

(iv) Although the "leaky" heading hold system was not correctly tested, it appears to possess some inherently undesirable features that increase the pilot work load in co-ordinating turns.

(v) A pitch stabilizer of the form tested resulted in very good longitudinal handling qualities, eliminating the heavy demand on pilot's attention inherent in the unstabilized aircraft at approach speeds.

## 8.0 ACKNOWLEDGMENTS

The assistance of the personnel of the Royal Aircraft Establishment, Bedford, England - in particular Mr. A. A. Woodfield and F/L J. F. Farley (now with Hawker-Siddeley) - in the preparation and enthusiastic execution of this program is gratefully acknowledged.

## 9.0 REFERENCES

1. Curry, P. R.; Johnston, J. A. — Operational V/STOL. Kestrel Tripartite Evaluation. SAE Paper 660320, Society of Automotive Engineers, April 1966.

2. Woodfield, A. A. — Theoretical Studies of Various Lateral and Directional Auto-Stabilizer Systems for a Jet V/STOL Aircraft (HS P1127) in Jet-Borne Flight. To be published.

3. Woodfield, A. A.; Farley, J. F. — In-Flight Simulation of Various Lateral and Directional Auto-Stabilizer Systems for a Jet V/STOL Aircraft (HS P1127) in Jet-Borne Flight. To be published.

| | | |
|---|---|---|
| 4. | Daw, D. F.<br>Lum, K.<br>McGregor, D. M. | Description of a Four Degrees of Freedom, V/STOL Aircraft, Airborne Simulator.<br>NRC, NAE Aero. Report LR-499, National Research Council of Canada, February 1968. |
| 5. | Gould, D. G. | The Model-Controlled Method for the Development of Variable Stability Aircraft.<br>NRC, NAE Aero. Report LR-345, National Research Council of Canada, June 1962. |
| 6. | Daw, D. F. | The NAE Airborne Flight Simulators.<br>Canadian Aeronautics and Space Journal, Vol. 11, 1965, pp. 97-102. |
| 7. | Etkin, B. | Dynamics of Flight: Stability and Control.<br>John Wiley and Sons, New York, 1959. |
| 8. | Smith, R. E. | A Comparison of V/STOL Aircraft Directional Handling Qualities Criteria for Visual and Instrument Flight Using an Airborne Simulator.<br>NRC, NAE Aero. Report LR-465, National Research Council of Canada, August 1966. |

TABLE 1

DIMENSIONAL STABILITY DERIVATIVES FOR THE HAWKER P1127

| LONGITUDINAL | | | | LATERAL-DIRECTIONAL | | | |
|---|---|---|---|---|---|---|---|
| DERIVATIVE | DIMENSION | 50 KNOTS | 80 KNOTS | DERIVATIVE | DIMENSION | 50 KNOTS | 80 KNOTS |
| $X_u$ | $\frac{ft/sec^2}{ft/sec}$ | -0.044 | -0.054 | $Y_\beta$ | $\frac{ft/sec^2}{rad}$ | -8.1 | -17.7 |
| $X_\alpha$ | $\frac{ft/sec^2}{rad}$ | -2.1 | -5.4 | $Y_r$ | $\frac{ft/sec^2}{rad/sec}$ | -0.27 | -0.27 |
| | | | | $Y_{\delta_r}$ | $\frac{ft/sec^2}{in}$ | -0.75 | -0.90 |
| $Z_u$ | $\frac{ft/sec^2}{ft/sec}$ | -0.026 | -0.016 | | | | |
| $Z_\alpha$ | $\frac{ft/sec^2}{rad}$ | -15.4 | -37.3 | $L_\beta$ | $\frac{rad/sec^2}{rad}$ | -1.0 | -1.9 |
| $Z_{\delta_T}$ | $\frac{ft/sec^2}{in}$ | -8.1 | -8.1 | $L_R$ | $\frac{rad/sec^2}{rad/sec}$ | +0.084 | +0.24 |
| $Z_{\delta_e}$ | $\frac{ft/sec^2}{in}$ | +0.055 | +0.14 | $L_P$ | $\frac{rad/sec^2}{rad/sec}$ | -0.81 | -1.29 |
| | | | | $L_{\delta_r}$ | $\frac{rad/sec^2}{in}$ | -0.041 | -0.103 |
| $M_u$ | $\frac{rad/sec^2}{ft/sec}$ | +0.0011 | +0.0018 | $L_{\delta_r'}$ | $\frac{rad/sec^2}{in}$ | +0.086 | +0.086 |
| $M_\alpha$ | $\frac{rad/sec^2}{rad}$ | +1.12 | +2.05 | $L_{\delta_a}$ | $\frac{rad/sec^2}{in}$ | +0.046 | +0.12 |
| $M_{\dot{\alpha}}$ | $\frac{rad/sec^2}{rad/sec}$ | -0.047 | -0.076 | $L_{\delta_a'}$ | $\frac{rad/sec^2}{in}$ | +0.50 | +0.50 |
| $M_q$ | $\frac{rad/sec^2}{rad/sec}$ | -0.19 | -0.27 | $N_\beta$ | $\frac{rad/sec^2}{rad}$ | -0.16 | -0.03 |
| $M_{\delta_e}$ | $\frac{rad/sec^2}{in}$ | +0.024 | +0.052 | $N_R$ | $\frac{rad/sec^2}{rad/sec}$ | -0.25 | -0.31 |
| $M_{\delta_e'}$ | $\frac{rad/sec^2}{in}$ | +0.18 | +0.18 | $N_P$ | $\frac{rad/sec^2}{rad/sec}$ | +0.021 | -0.033 |
| | | | | $N_{\delta_r}$ | $\frac{rad/sec^2}{in}$ | +0.030 | +0.077 |
| | | | | $N_{\delta_r'}$ | $\frac{rad/sec^2}{in}$ | +0.24 | +0.24 |
| | | | | $N_{\delta_a}$ | $\frac{rad/sec^2}{in}$ | 0 | +0.0014 |
| | | | | $N_{\delta_a'}$ | $\frac{rad/sec^2}{in}$ | -0.0084 | -0.0084 |

BLANK PAGE


FIG. 1 AIRBORNE V/STOL SIMULATOR

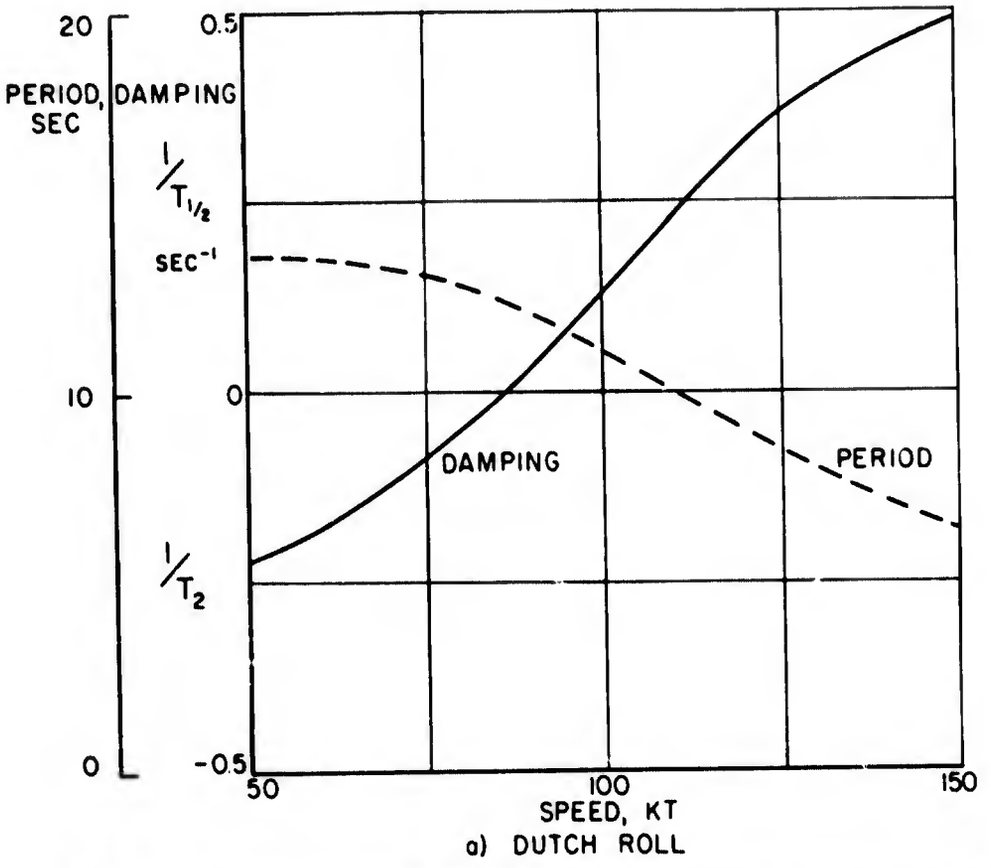


a) DUTCH ROLL

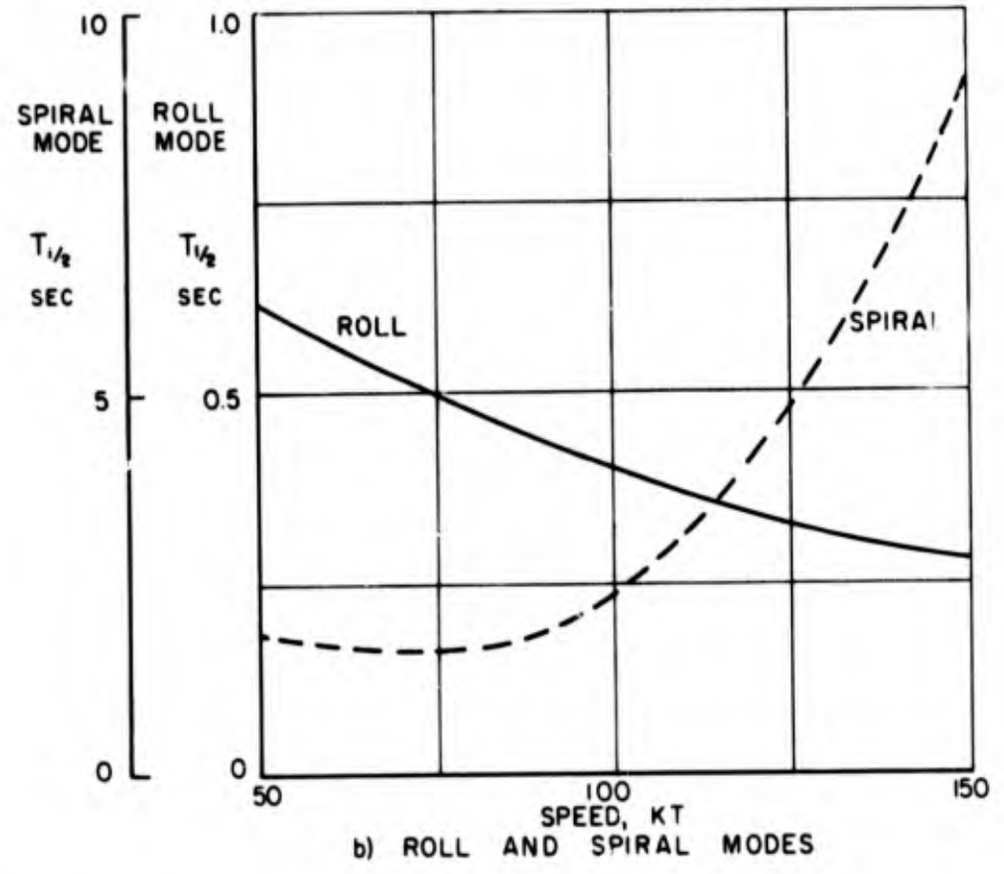


b) ROLL AND SPIRAL MODES

FIG. 2
BASIC P1127 LATERAL-DIRECTIONAL MODAL CHARACTERISTICS

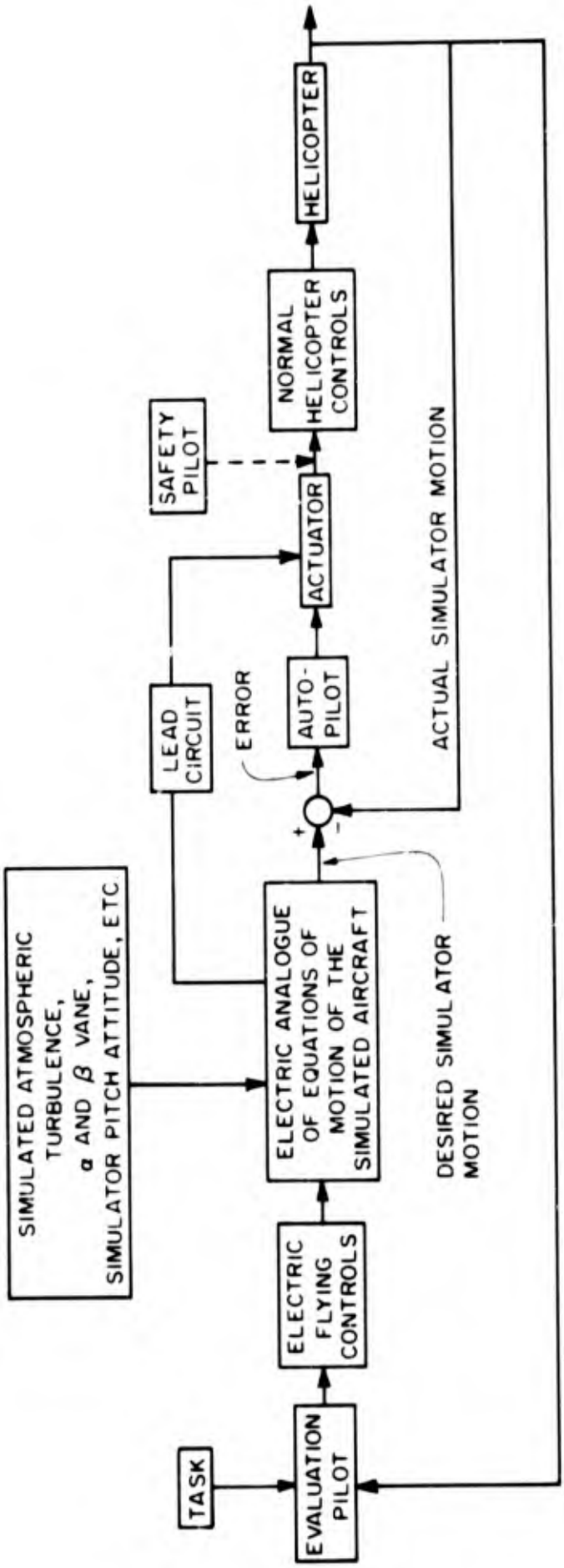


FIG. 3 "MODEL-CONTROLLED" SIMULATION METHOD

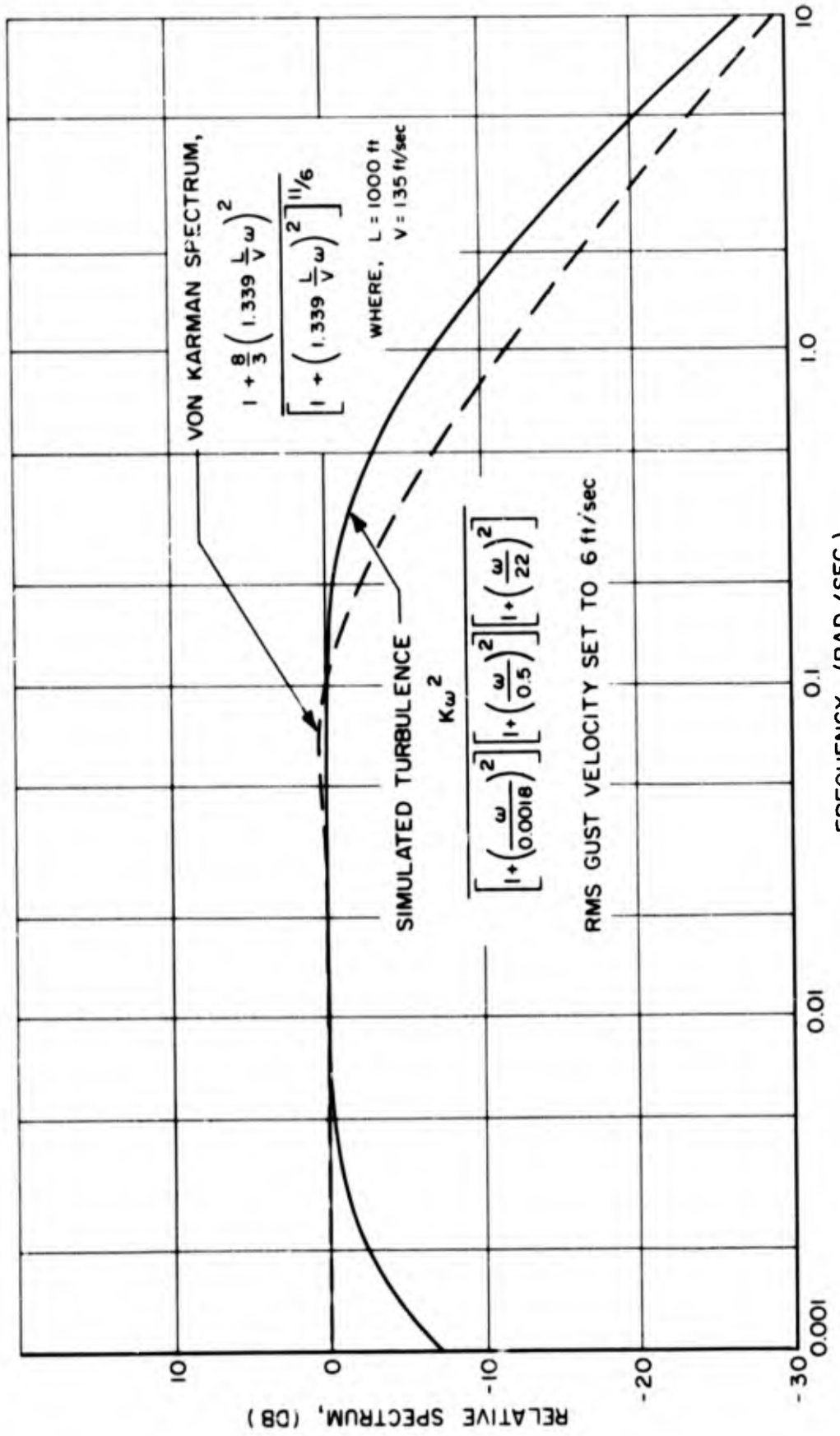


FIG. 4 POWER SPECTRUM OF SYNTHETIC TURBULENCE GENERATOR

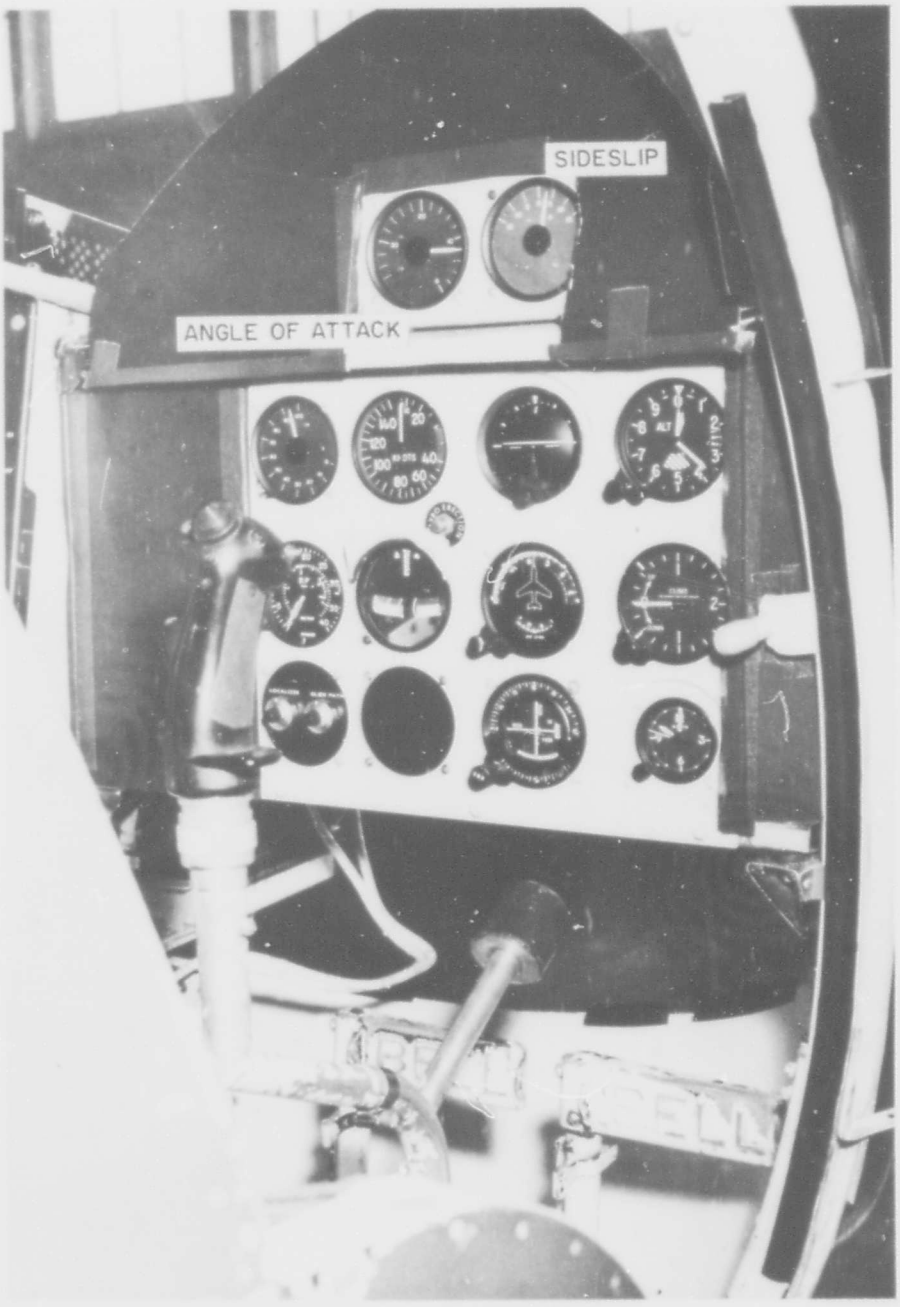


FIG. 5 INSTRUMENT PANEL ARRANGEMENT
FOR VISUAL FLIGHTS

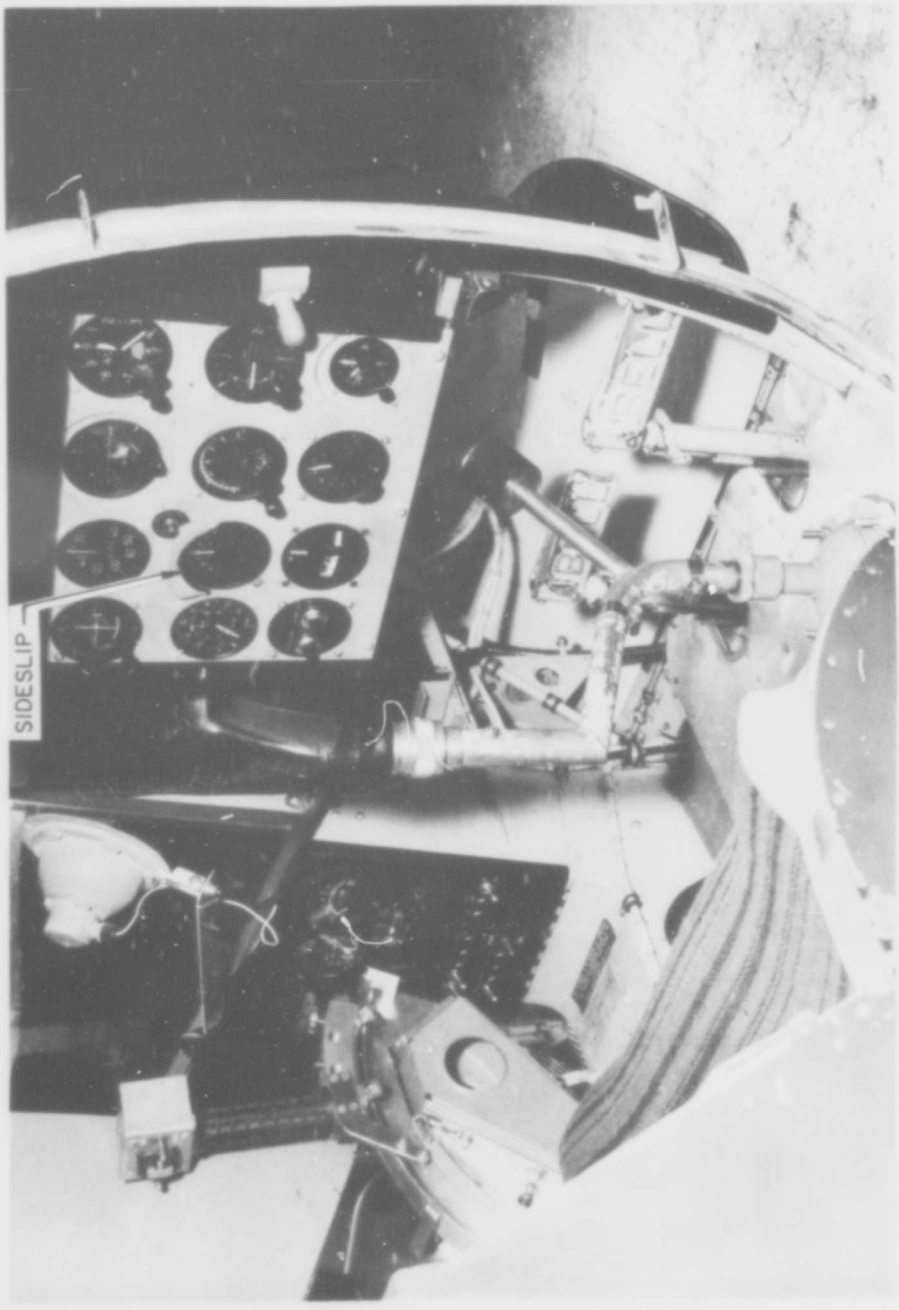


FIG. 6 COCKPIT LAY-OUT FOR INSTRUMENT FLIGHTS

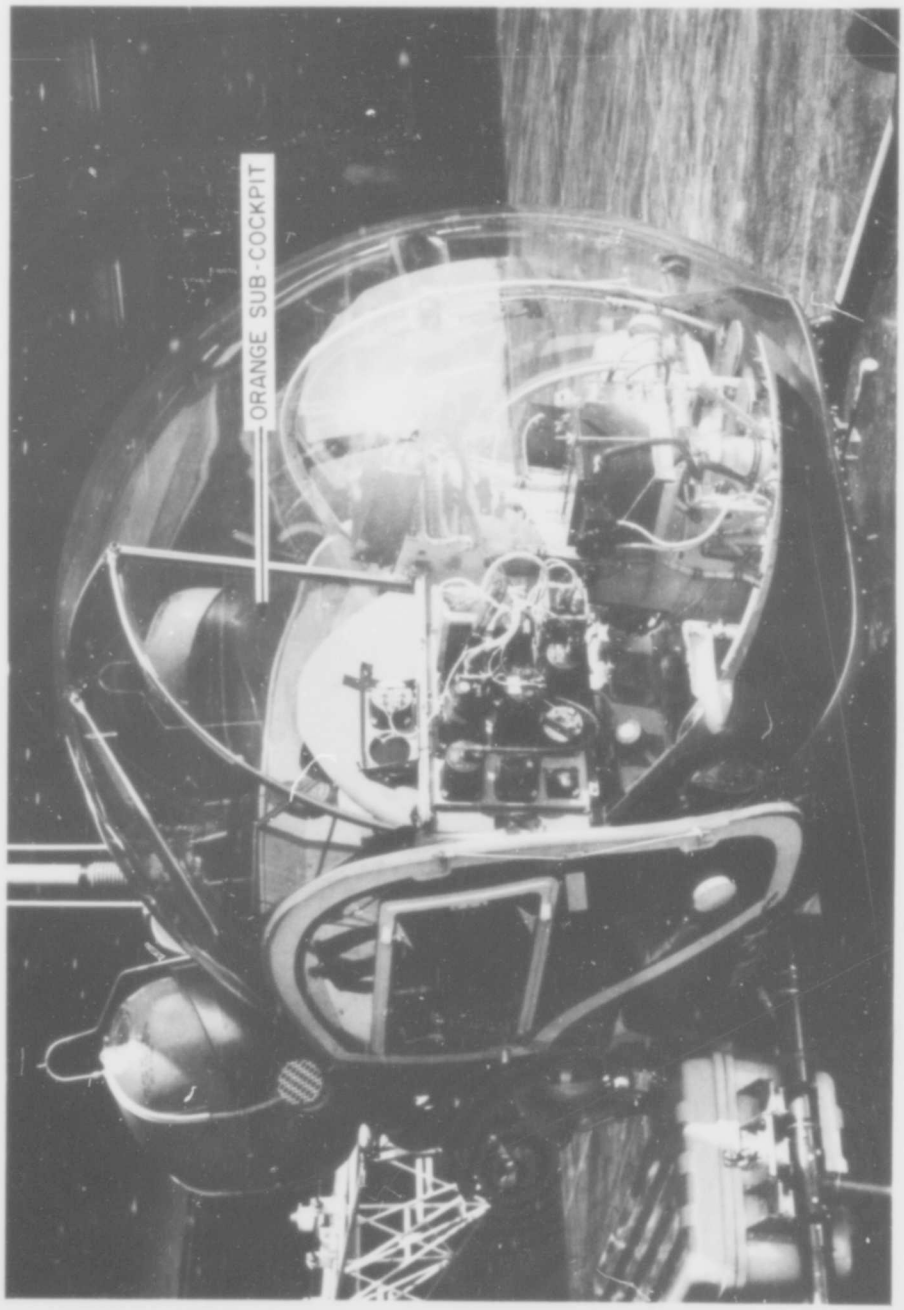


FIG. 7 ORANGE SUB-COCKPIT INSTALLATION

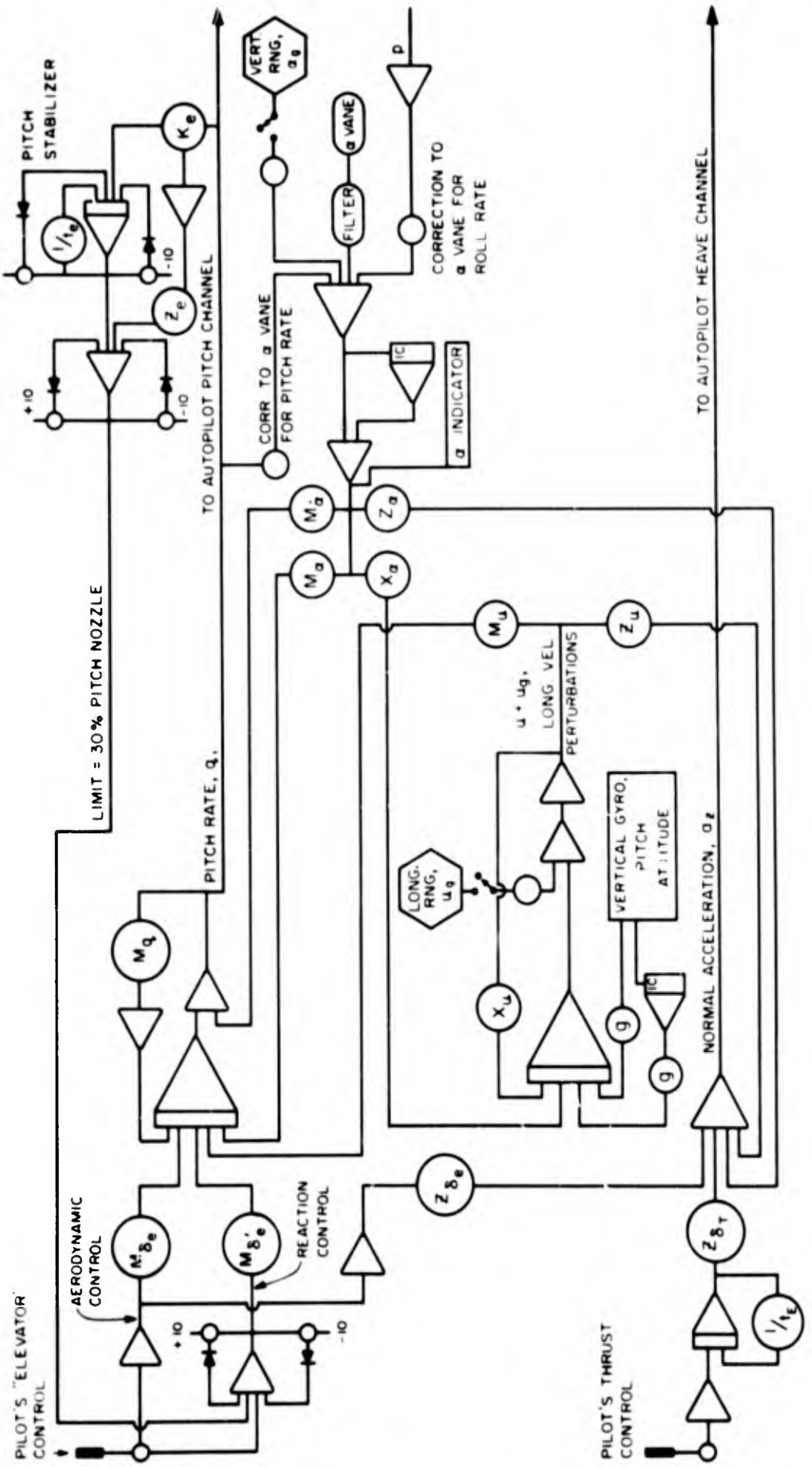


FIG. 8 ANALOGUE CIRCUIT FOR THE PI127 LONGITUDINAL EQUATIONS OF MOTION

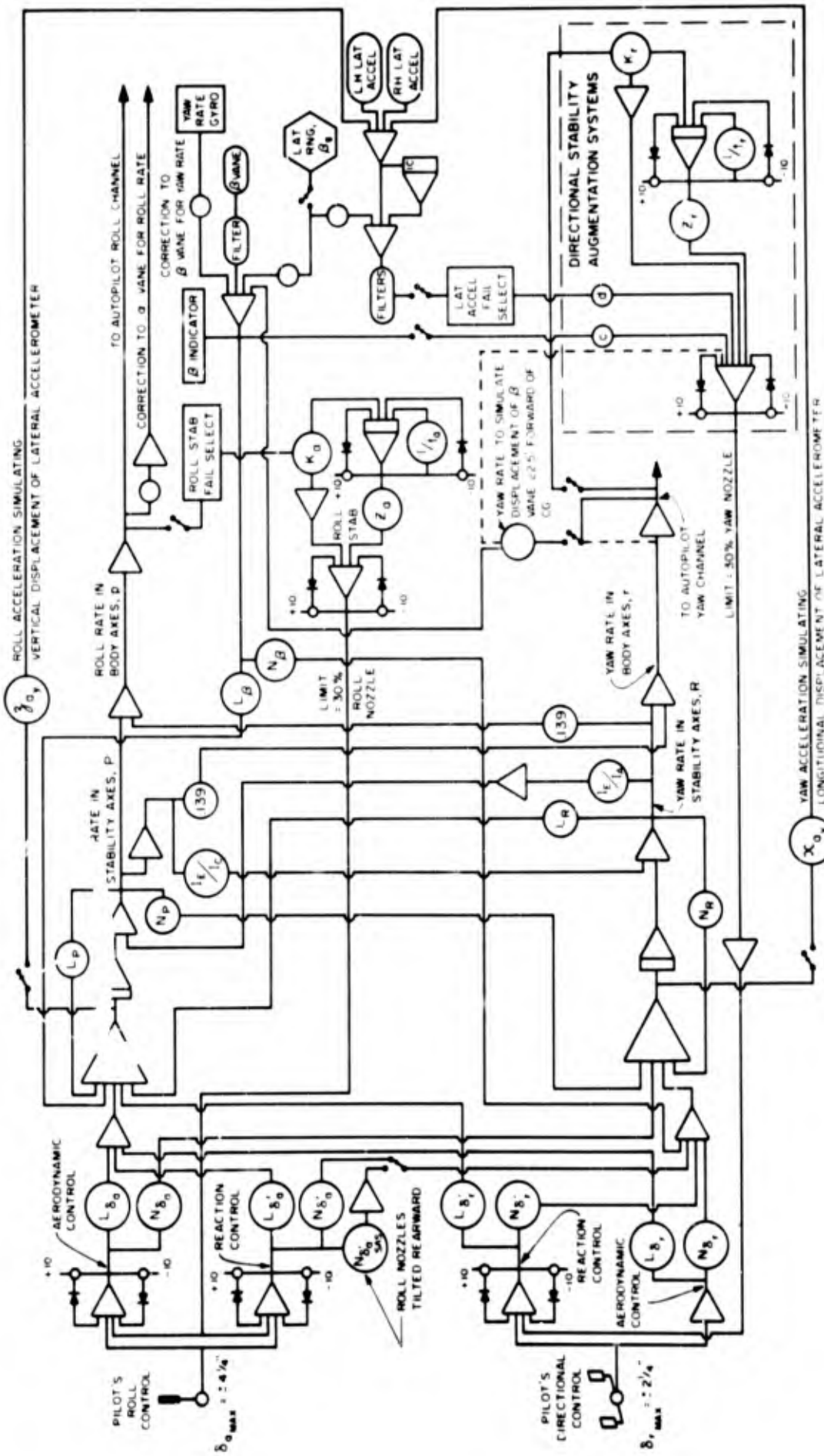


FIG. 9 ANALOGUE CIRCUIT FOR THE PI127 LATERAL-DIRECTIONAL EQUATIONS OF MOTION